CHEMICAL ENGINEERING TRANSACTIONS
VOL. 89, 2021
A publication of AIDIC
The Italian Association of Chemical Engineering
Online at www.cetjournal.it
Guest Editors: Jeng Shiun Lim, Nor Alafiza Yunus, Jiří Jaromír Klemeš

ISBN 978-88-95608-87-7; **ISSN** 2283-9216
DOI: 10.3303/CET2189096

Facile Synthesis of MAX Modified Graphitic Carbon Nitride Nanocomposite for Stimulating Hydrogen Production Through Photocatalytic Water Splitting

Muhammad Tahir*, Areen Sherryna, Zaki Yamani Zakaria

Department of Chemical Reaction Engineering, School of Chemical and Energy Engineering, Universiti Teknologi Malaysia, 81310, UTM, Johor Bahru, Johor, Malaysia.
m.tahir@utm.my/bttahir@yahoo.com

Photocatalytic hydrogen production has been considered a promising strategy for developing green, sustainable, and clean energy resources to substitute non-renewable fossil fuels. A widely studied graphitic carbon nitride (g-C_3N_4) has garnered research attention due to their commercial availability and excellent photochemical efficiency to drive hydrogen generation through water splitting process. Undesirable recombination of photocarriers, higher electrostatic potential barriers, and low solar absorbance in a single g-C_3N_4 photocatalyst impede their efficiency in the energy conversion field. Several alternatives have been proposed over decades to improve the photocatalytic efficiency of g-C_3N_4. Among them, noble metal integration has been denoted as the most promising technique to maximize solar efficiency. Less availability and non-economical, however, limit their functionality surpasses their unique SPR characteristics. In this study, a novel composite of V_2AlC MAX/g-C_3N_4 that exhibits the same functionality as those of noble metals was fabricated via a sol-gel method, and their efficiency enhancement was investigated using a liquid slurry photoreactor system. The optimal 10% loading of V_2AlC exhibits maximum hydrogen generation up to 196.25 μmol g^{-1} h^{-1}, which is 2.8-fold higher than pure g-C_3N_4. The photoactivity enhancement observed was due to the intimate contact formed between V_2AlC with g-C_3N_4, accelerating the migration of the photogenerated charges. The electrons confinement due to the induced Schottky junction hamper the recombination of and maximizes the separation of the photocarriers. The prepared sample was characterized by XRD, PL analysis, and SEM. The successful integration of V_2AlC with g-C_3N_4 was affirmed by XRD analysis as the characteristics peaks of both materials are present in the composite. The stacked irregular structure of V_2AlC/g-C_3N_4 highly indicates that a tight interface contact was formed between both semiconductors. This study provides new insight into newly developed V_2AlC MAX-based g-C_3N_4 for clean energy systems and unravels their potential in solar energy applications.

1. Introduction

Hydrogen energy has been regarded as the best alternative to substitute fossil fuels as a prime energy carrier, specifically for electricity generation and transportation. It was denoted that current conventional techniques which utilize fossil fuels to generate a large scale of H_2 gas, such as Steam Methane Reforming (STM) and water-gas shift reaction, are typically associated with higher energy inputs and carbon footprints emission (Chen et al., 2020). Photocatalytic water splitting by scavenging energy from the sunlight using semiconductor materials was considered as a propitious maneuver for generating a clean and renewable H_2 gas. In recent advancements, the study on photocatalytic H_2 production has been greatly extended by utilizing various kinds of semiconductors composite. A recent study by Vaiano et al. (2021) disclosed that hydrogen generation was significantly induced up to 560.5 μmol L^{-1} h^{-1} from the glucose solution by utilizing Ni/$LaFeO_3$ composite. In different studies, Basaleh and Mahmoud (2021) ascribed that the composite of $CoAl_2O_4$−g-C_3N_4 substantially promotes the isolation of the photogenerated charge carriers with an improved hydrogen generation rate. Xu et al. (2021) disclosed that the heterojunction formation between g-C_3N_4/Ti_3C_2 MXene favors hydrogen production and enhanced photocatalytic activity. The construction of Z-scheme heterojunction in the composite of g-

Paper Received: 2 May 2021; Revised: 14 September 2021; Accepted: 25 November 2021
Please cite this article as: Tahir M., Sherryna A., Zakaria Z.Y., 2021, Facile Synthesis of MAX Modified Graphitic Carbon Nitride Nanocomposite for Stimulating Hydrogen Production Through Photocatalytic Water Splitting, Chemical Engineering Transactions, 89, 571-576 DOI:10.3303/CET2189096

C_3N_4/TiO_2/CQDs/Au remarked an enhancement in the photocatalytic hydrogen production due to stronger redox activity and proficient charges transfer. Graphitic carbon nitride (g-C_3N_4) gained enormous reputability as a single and hybrid photocatalyst due to their abundancy, excellent photochemical properties, and commercial availability. Despite their beneficial attribution in the photocatalysis field, it was reported that the electrostatic potential barrier in g-C_3N_4 favors the recombination of the photocarriers leading to the restriction in the redox activity (Zhang et al., 2021). Lower solar absorbance exhibit by g-C_3N_4 impedes their role as an individual photocatalyst for water splitting. V_2AlC, which belongs to the family of MAX phases, gained scientific interests over their excellent electrical conductivity and good optical properties (Schneider et al., 2006). Semiconductors with higher conductivity could maximize the utilization of light and facilitate photoexcitation. The presence of vanadium (V) metal in V_2AlC substantially improves the conductivity and induces the Schottky barrier formation at the metal-semiconductor interfaces (Varma et al., 2018). It was noted that hybridizing g-C_3N_4 with V_2AlC could overcome the shortcomings of a single g-C_3N_4 photocatalyst, augmenting the photocatalytic performance. Highly metallic V_2AlC could substitute the non-commercial noble metals and serves as trapping centres to confine electrons from recombined with holes at the semiconductor counterpart. Limited research has focused on the photoactivity enhancement by utilizing the MAX phase as a co-catalyst, while none has been reported on the utilization of V_2AlC in photocatalytic hydrogen production. A novel two-dimensional V_2AlC/g-C_3N_4 composite has been fabricated via a sol-gel method, and their photocatalytic enhancement towards hydrogen generation has been investigated.

2. Experimental Section

2.1 Materials

Melamine (Sigma Aldrich, AR ≥ 99 %) for the synthesis of bulk g-C3N4, V_2AlC (Sigma Aldrich), Methanol (Merck, AR ≥ 99 %).

2.2 Synthesis of g-C_3N_4 nanosheets

Bulk g-C_3N_4 was prepared through the hydrothermal approach by using melamine as the precursor. Typically, 5 g of melamine was placed in a crucible, covered with a lid, and heated up for 2 h at 550 °C inside the furnace. The obtained yellow colored bulk was then ground into a fine powder using mortar and pestle. The yellow powder of g-C_3N_4 was dispersed in methanol and stirred for 2 h, under air atmosphere at normal temperature, before drying in the oven for 24 h at 100 °C, named g-C_3N_4 nanosheets.

2.3 Synthesis of V_2AlC/g-C_3N_4

The composite of V_2AlC/g-C_3N_4 sample was prepared via sol-gel method at room temperature. 0.5 g of g-C_3N_4 (sample A) and 0.025 g amount of V_2AlC (sample B) was dispersed in 20 mL of methanol and stirred for 2 h, under open environment at normal temperature. The uniformly dispersed sample B was added to sample A and stirred for another 2 h to ensure homogeneous dispersion of both samples. The obtained sample was dried in the oven at 100 °C under airflow for overnight, named V_2AlC/g-C_3N_4 composite. Different samples of V_2AlC/g-C_3N_4 with different V_2AlC loading (5 %, 10 %, 15 %, 20 %) were prepared following the same steps. Different samples of V_2AlC/g-C_3N_4 was denoted as 5 % V_2AlC/g-C_3N_4, 10% V_2AlC/g-C_3N_4, 15% V_2AlC/g-C_3N_4, and 20% V_2AlC/g-C_3N_4.

2.4 Characterization

The crystal structure was investigated using X-ray diffractometer (D/teX Ultra 250 Smart Lab), operated at 40 kV and 30 mA over the range 2-θ of 3° to 100° and speed of 8.255 °min^{-1}. The photoluminescence (PL) measurements were conducted using a HORIBA Scientific spectrophotometer operated at the wavelength of 325 nm. The morphologies and microstructures analysis was performed using scanning electron microscopy (SEM, Hitachi SU8020).

2.5 Photoactivity Test

The photocatalytic activity test was carried out using a liquid slurry photoreactor system equipped with a 35 W HID Xe Lamp (λ = 420 nm) with an intensity of 12,000 K as a visible light source. Specifically, 0.1 g of the photocatalyst was dispersed in a solution containing a mixture of 95 mL distilled water and 5 mL (5 %) vol of methanol as a sacrificial agent under continuous magnetic stirring. Nitrogen gas (N_2) was supplied to the reactor system to purge out air and impurities inside the system for 30 mins. After the reactor system was cleaned from other impurities, the lamp was turned on, and a hydrogen sampling bag was connected to the system under a continuous flow of N_2 gas regulated at 15 mL min^{-1}. The concentration of H_2 gas was measured every 1 h for a duration of 4 h and analyzed using a hydrogen gas analyzer manufactured by Brotie Technology (Brotie Model 100).

3. Results and Discussion

3.1 Characterization of Samples

XRD analysis has been performed to validate the crystal structure of the prepared samples and to determine the successful fabrication of the $V_2AlC/g\text{-}C_3N_4$ composite. The intense peak at 13.42 ° and 41 ° in Figure 1a are ascribed to the MAX phase of V_2AlC based on the previous literature (Gorshkov et al., 2020). The sharp peak inherently indicates the higher crystallinity structure of V_2AlC. A pronounced peak at 13.1 ° and 27.3 °, corresponding to (001) and (002) facets, signifies the structural packing and interplanar stacking of $g\text{-}C_3N_4$. The diffraction peaks are in accordance with JCPDS No. 87-1526. For 10 % $V_2AlC/g\text{-}C_3N_4$, both characteristics peaks of $g\text{-}C_3N_4$ and V_2AlC are present, indicating a successful integration.

PL test has been performed on the samples to acquire details on the photocarriers separation efficiency with corresponding results shown in Figure 1b. Typically, lower intensity highly indicates an efficient separation of the electron-hole pairs. It was noted that higher separation of the photoinduced charges profoundly impacts the photocatalytic performances. It can be observed that the composite of $V_2AlC/g\text{-}C_3N_4$ exhibits a higher peak depression with lower intensity compared to pure $g\text{-}C_3N_4$. Higher PL intensity by $g\text{-}C_3N_4$ was believed due to higher recombination rates of the photogenerated charges. On the other hand, V_2AlC does not show any prominent peaks due to their metallic nature and non-semiconducting properties. It was further affirmed that the formation of the Schottky barrier induced by highly conductive V_2AlC notably confines the electrons and prevents the backward recombination of the charge carriers. The trapped electrons at the V_2AlC surfaces and holes at the $g\text{-}C_3N_4$ are spatially separated, elucidate the lower intensity peak observed in $V_2AlC/g\text{-}C_3N_4$.

The morphological structure of pristine $g\text{-}C_3N_4$, V_2AlC, and composite of 10 % $V_2AlC/g\text{-}C_3N_4$ were investigated using SEM analysis. As denoted in Figure 2a, pristine $g\text{-}C_3N_4$ synthesized through the thermal decomposition of melamine exhibits irregular clumps with compact crumple sheet morphology, where the sheets of the $g\text{-}C_3N_4$ can be observed to be agglomerated and stacked onto each other. Whereas V_2AlC in Figure 2b shows a prominent non-exfoliated MAX phase suggesting that aluminum was attached at the layered V_2AlC as they exhibit a compact, dense structure (Hu et al., 2008). The successful integration of $g\text{-}C_3N_4$ with V_2AlC can be observed in Figure 2c, as it was evident that the smooth surfaces of V_2AlC were covered with the irregular structure of $g\text{-}C_3N_4$, forming an intimate contact with each other. Close interfaces contact between $g\text{-}C_3N_4$ and V_2AlC promotes an efficient transfer of photocarriers as shorter electrons transmission and lower transfer resistances can be achieved.

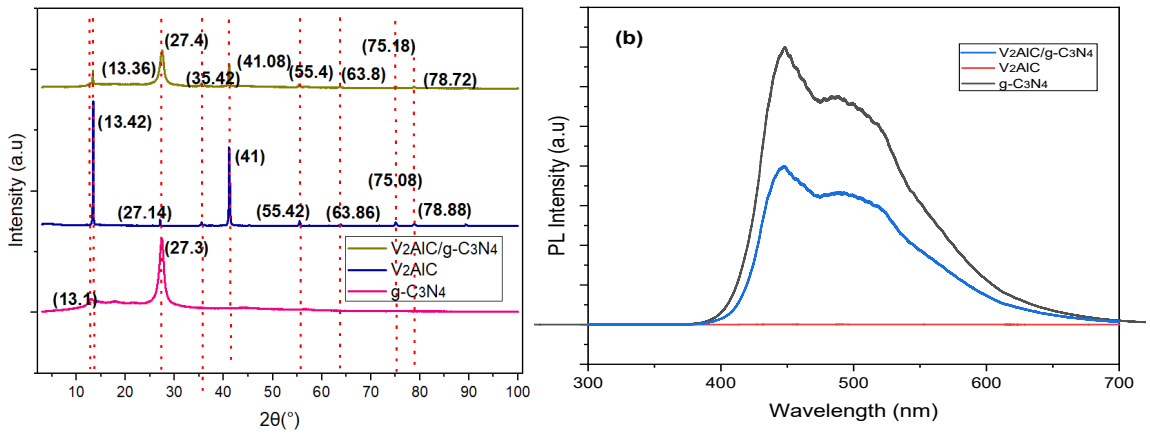

Figure 1: (a) XRD patterns (b) PL analysis of pristine $g\text{-}C_3N_4$, V_2AlC and composite of 10 % $V_2AlC/g\text{-}C_3N_4$

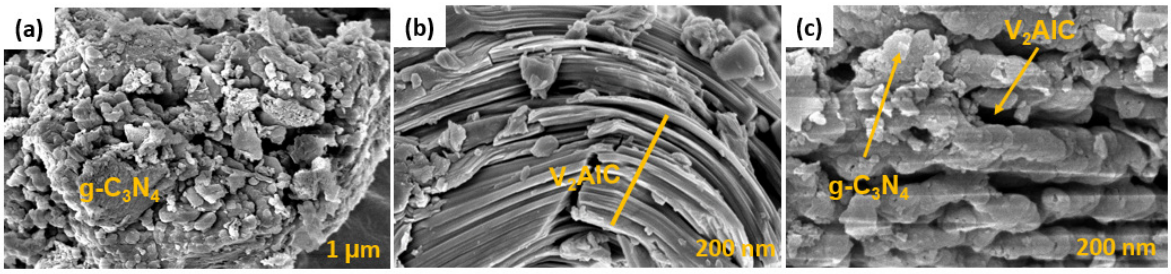

Figure 2: SEM images of (a) pristine $g\text{-}C_3N_4$, (b) V_2AlC, and (c) composite of 10 % $V_2AlC/g\text{-}C_3N_4$

3.2 Bandgap of g-C_3N_4 and V_2AlC/g-C_3N_4

The energy band gap of g-C_3N_4 and V_2AlC/g-C_3N_4 were estimated from the Tauc plot and calculated based on Kubelka−Munk (KM) function through the relationship between $(\alpha hv)^2$ and photon energy Tauc plots. As indicated in Eq(1), α was referred to as the absorption coefficient of the material, while r was defined as the nature of the semiconductor. The band energies of 2.95 eV and 2.84 eV were obtained for g-C_3N_4 and V_2AlC/g-C_3N_4, respectively. The band gap energies obtained suggest that the addition of V_2AlC does not significantly impact the band gap of the g-C_3N_4. The relationship between E_g, CB and VB is denoted in Eq(2), while the CB calculation can be obtained from Eq(3) by which coefficient X stands for semiconductor electronegativity (EN), E was denoted as energy-free electron, and E_g is the band gap of semiconductor.

$$E_g = (\alpha hv)^{\frac{1}{r}} \quad (1)$$

$$E_g = VB - CB \quad (2)$$

$$CB = X - E - 0.5E_g \quad (3)$$

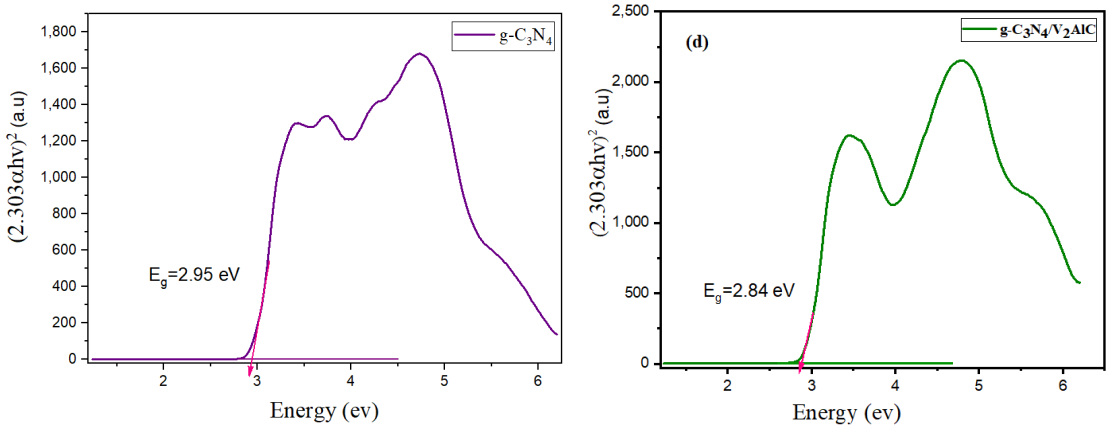

Figure 3: Tauc plot of (a) pristine g-C_3N_4, (b) composite of 10 % V_2AlC/g-C_3N_4

3.3 Photocatalytic Hydrogen Production

The photocatalytic performances of pristine g-C_3N_4, V_2AlC and V_2AlC/g-C_3N_4 with different percentage loading of V_2AlC (5 %, 10 %, 15 %, 20 %) are demonstrated in Figure 4a. The obtained results were calculated as according to Eq(4) :

$$\text{Yield}\left(\frac{\mu\text{mol}}{\text{g of catalyst}}\right) = A\left(\text{ppm}\left(\frac{\text{mg}}{\text{L}}\right)\right) \times V\,(\text{mL}) \times \frac{C_1\,(1\text{L})}{1{,}000\ \text{mL}} \times \frac{M\,(1\ \text{mol})}{2{,}000\ \text{mg}} \times \frac{C_2\,(10^6\ \mu\text{mol})}{1\ \text{mol}} \times \frac{\text{Catalyst weight}}{\text{mass of } V_2AlC/g{-}C_3N_4\,(\text{g})} \quad (4)$$

Where A is the hydrogen yield in ppm, V denotes as the volume of the liquid, 2,000 is the molecular weight of hydrogen gas in mg. C_1 stands for the conversion unit from mL to L, and C_2 stands for the conversion from mol to µmol. M is the molecular weight of hydrogen in mg/mol.

It is apparent that H_2 generation is improved on V_2AlC/g-C_3N_4 composite compared to pristine g-C_3N_4. Pristine g-C_3N_4 exhibited poor H_2 generation performances with the H_2 rate of 70 µmol g^{-1} h^{-1}. The enhancement in the photocatalytic activity is highly attributed to the improved solar absorption and optical performances by the composites. It was noted that the formation of intimate contact between g-C_3N_4 and V_2AlC substantially accelerating the migration of the photogenerated charges due to the shorter transmission pathway (Reli et al., 2021). The integration of highly conductive V_2AlC renders them with an electron sink functionality, resulting in Schottky barrier formation at the metal-semiconductor interfaces. The formation of Schottky barrier improves the separation of the photogenerated charges as they confine the electrons at the V_2AlC surfaces and inhibit them from recombining with holes at the semiconductor counterpart, astoundingly improve the photocatalytic performances. It can be observed that the composite with 10 % loading of V_2AlC exhibits the highest hydrogen generation rate of 196.25 µmol g^{-1} h^{-1}, which is 2.8-fold higher than pristine g-C_3N_4. On the other hand, excessive loading of V_2AlC results in a declined photoactivity, probably due to the light-shielding effects which hinder the absorption of light on g-C_3N_4 (Su et al.,2019). The optimal control of 10 % V_2AlC loading could hamper their accumulation on the semiconductor counterpart, favoring light to reach the semiconductor surface for photon absorption. It was noted that 10 % loading could maximize the efficiency by optimally activates the surface of g-

C_3N_4 and provide sufficient catalytic active sites for driving the redox reaction. It can also be ascribed that transitional element V from V_2AlC, which exhibits a higher work function, is believed to be responsible for their highly conductive properties and one of the key criteria for fostering hydrogen generation (Mendeza et al., 2021). The utilization of MAX phases with g-C_3N_4 in the current study shows a substantial catalytic improvement with better efficiency than those reported by noble metals/g-C_3N_4 and other hybrid composites. The maximum rate of hydrogen generation of the prepared V_2AlC/g-C_3N_4 is far better than Ag_3PO_4/Ag/g-C_3N_4 (4 μmol g^{-1} h^{-1}) (You et al., 2017), g-C_3N_4/Ag/MoS_2 (100 μmol g^{-1} h^{-1}) (Lu et al., 2017), and WS_2/g-C_3N_4 (154 μmol g^{-1} h^{-1}) (Zhou et al., 2019).

3.4 Mechanism

The charge transfer mechanism of the V_2AlC/g-C_3N_4 composite is demonstrated in Figure 4b. It can be explicated that the difference in the work function between metallic V_2AlC and g-C_3N_4 promotes the transfer of electrons towards V_2AlC. The photocatalytic mechanism will be as follows: Under the irradiation of light, the photogenerated charges will be generated at the valence band (VB) of g-C_3N_4 as shown in Eq(5), and the photogenerated electrons will be excited to the conduction band (CB) after the photon absorption, leaving holes in the VB. V_2AlC serves as electron acceptors as they exhibit a higher work function typically associated with a lower Fermi level than g-C_3N_4. It was noted that pristine g-C_3N_4 exhibit a work function of 3.81 eV (Yang et al., 2020), while V_2AlC having a work function of 4.3 eV (Pinek et al., 2018). Therefore, the electrons will migrate from a higher Fermi level of g-C_3N_4 towards the lower Fermi level of V_2AlC until their Fermi levels attain an equilibrium by which the electrons will be trapped at V_2AlC as shown in Eq(6) (Khan et al., 2020). The strong interfacial charges at metal-semiconductor interfaces inducing the Schottky barrier confining the electrons from returning to the semiconductor counterpart and recombining with holes (Tahir, 2021). The holes that remained at the VB of g-C_3N_4 will undergo oxidation reaction with water to produce H^+ and also will be consumed by sacrificial reagent (methanol) as denoted in Eq(7) – (8). The accumulated electrons at the V_2AlC surfaces will undergo a reduction reaction with H^+ to generate H_2 as shown in Eq(9).

$$g - C_3N_4 + hv \rightarrow g - C_3N_4\ (e^- + h^+) \quad (5)$$

$$g - C_3N_4(e-) + V_2AlC \rightarrow V_2AlC(e-) \quad (6)$$

$$H_2O + h^+ \rightarrow \frac{1}{2} O_2 + 2H^+ \quad (7)$$

$$CH_3OH + 2h^+ \rightarrow CH_2O + 2H^+ \quad (8)$$

$$2e^- + 2H^+ \rightarrow H_2 \quad (9)$$

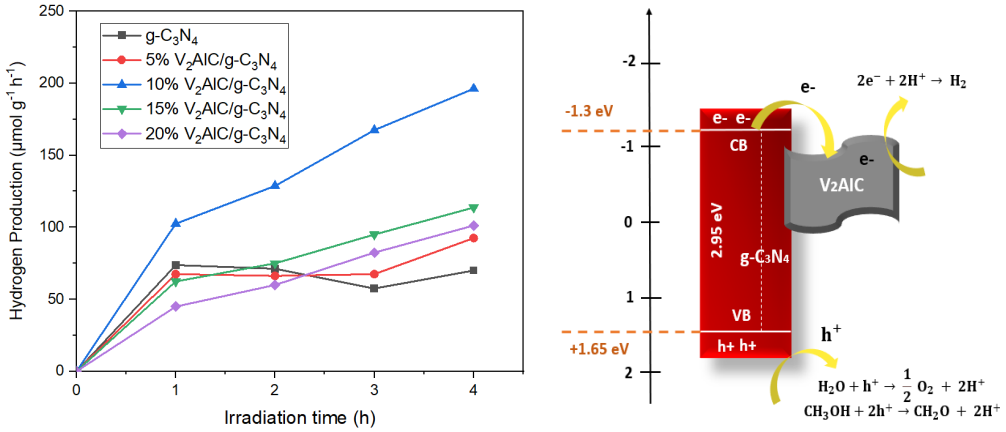

Figure 4: (a) The rate of hydrogen generation for pristine g-C_3N_4 and V_2AlC/g-C_3N_4 composite with different V_2AlC loading, (b) photocatalytic electron transfer mechanism in V_2AlC/g-C_3N_4 composite

4. Conclusion

The composite of V_2AlC/g-C_3N_4 was successfully fabricated via the sol-gel method, and their photocatalytic efficiency was tested under visible light irradiation. Hydrogen production was observed to escalate up to 196.25 μmol g^{-1} h^{-1} after 10 % V_2AlC was introduced, which is 2.8-fold higher than pristine g-C_3N_4. Higher photocatalytic performances observed can be attributed to the following: (1) introduction of V_2AlC induced Schottky barrier which suppressed the recombination and imparted a facile separation of the photocarriers; (2) proficient charges

transfer due to intimate contact formed between the metal-semiconductor, shortening the transmission pathway; (3) presence of V_2AlC rendered extra catalytic active sites promoting the redox reaction. This work provides new insight into newly developed V_2AlC MAX-based g-C_3N_4 for clean energy systems and to unravel their potential in solar energy applications.

Acknowledgement

The authors would like to extend their most profound appreciation to Ministry of Higher Education for the financial support under Fundamental Research Grant Scheme (FRGS, R.J130000.7851.5F384).

References

Basaleh A., Mahmoud M.H.H., 2021, $CoAl_2O_4$-g-C_3N_4 Nanocomposite Photocatalysts for Powerful Visible-Light-Driven Hydrogen Production, ACS Omega, 6(15), 10428-10436.

Chen W.T., Dong Y., Yadav P., Aughterson R.D., Sun-Waterhouse D., Waterhouse G.I.N., 2020, Effect of Alcohol Sacrificial Agent on the Performance of Cu/TiO_2 photocatalysts for UV-driven Hydrogen Production, Applied Catalysis A: General, 602, 117703-117719.

Gorshkov V.A., Karpov A.V., Kovalev D.Y., Sychev A.E., 2020, Synthesis, Structure, and Properties of Material Based on V_2AlC MAX Phase, Physics of Metals and Metallography, 121(8), 765-771.

Hu C., He L., Liu M., Wang X., Wang J., Li M., Bao Y., Zhou Y., 2008, In Situ Reaction Synthesis and Mechanical Properties of V_2AlC, Journal of the American Ceramic Society, 91(12), 4029-4035.

Khan A.A., Tahir M., Bafaqeer A., 2020, Constructing a Stable 2D Layered Ti_3C_2 MXene Cocatalyst-Assisted TiO_2/g-C_3N_4/Ti_3C_2 Heterojunction for Tailoring Photocatalytic Bireforming of Methane under Visible Light, Energy & Fuels, 34(8), 9810-9828.

Lu D., Wang H., Zhao X., Kondamareddy K.K., Ding J., Li C., Fang P., 2017, Highly Efficient Visible-Light-Induced Photoactivity of Z-Scheme g-C_3N_4/Ag/MoS_2 Ternary Photocatalysts for Organic Pollutant Degradation and Production of Hydrogen, ACS Sustainable Chemistry & Engineering, 5(2), 1436-1445.

Mendeza M.S., Lemarchanda A., Traorea M., Amara M.B., Perruchotb C., Nikravecha M., Kanaeva A., 2021, Preparation and Photocatalytic Activity of Coatings based on Size-selective V-TiO_2 Nanoparticles, Chemical Engineering Transactions, 84, 19-24.

Pinek D., Ito T., Ikemoto M., Nakatake M., Ouisse T., 2018, Electronic structure of V_2AlC, Physical Review B, 98(3), 1-9.

Reli M., Ambrožová N., Valášková M., Edelmannová M., Čapek L., Schimpf C., Motylenko M., Rafaja D., Kočí, K., 2021, Photocatalytic water splitting over CeO_2/Fe_2O_3/Ver photocatalysts, Energy Conversion and Management, 238.

Schneider J. M., Mertens R., Music D., 2006, Structure of V_2AlC studied by theory and experiment, Journal of Applied Physics, 99(1), 1-4.

Su T., Hood Z. D., Naguib M., Bai L., Luo S., Rouleau C. M., Ivanov I. N., Ji H., Qin Z., Wu Z., 2019, Monolayer $Ti_3C_2T_x$ as an Effective Co-catalyst for Enhanced Photocatalytic Hydrogen Production over TiO_2, ACS Applied Energy Materials, 2(7), 4640-4651.

Tahir M., 2021, Investigating the Influential Effect of Etchant Time in Constructing 2D/2D HCN/MXene Heterojunction with Controlled Growth of TiO_2 NPs for Stimulating Photocatalytic H_2 Production, Energy & Fuels, 35(8), 6807-6822.

Varma R., Yadav M., Tiwari K., Makani N., Gupta S., Kothari D.C., Miotello A., Patel N., 2018, Roles of Vanadium and Nitrogen in Photocatalytic Activity of VN-Codoped TiO_2 Photocatalyst, Photochem Photobiol, 94(5), 955-964.

Yang C., Tan Q., Li Q., Zhou J., Fan J., Li B., Sun J., Lv K., 2020, 2D/2D Ti_3C_2 MXene/g-C_3N_4 Nanosheets Heterojunction for High Efficient CO_2 Reduction Photocatalyst: Dual Effects of Urea, Applied Catalysis B: Environmental, 268, 118738-118748.

You M., Pan J., Chi C., Wang B., Zhao W., Song C., Zheng Y., Li, C., 2017, The Visible Light Hydrogen Production of the Z-Scheme Ag_3PO_4/Ag/g-C_3N_4 Nanosheets Composites, Journal of Materials Science, 53(3), 1978-1986.

Zhang M., Lai C., Li B., Xu F., Huang D., Liu S., Qin L., Liu X., Yi H., Fu Y., Li L., An N., Chen L., 2021, Insightful Understanding of Charge Carrier Transfer in 2D/2D Heterojunction Photocatalyst: Ni-Co Layered Double Hydroxides Deposited on Ornamental g-C_3N_4 Ultrathin Nanosheet with Boosted Molecular Oxygen Activation, Chemical Engineering Journal, 422, 130120-130131.

Zhou Y., Ye X., Lin D., 2019, One-pot Synthesis of Non-noble Metal WS_2/g-C_3N_4 Photocatalysts with Enhanced Photocatalytic Hydrogen Production, International Journal of Hydrogen Energy, 44(29), 14927-14937.